Astron. Astrophys. 263, 87–96 (1992)

ASTRONOMY AND ASTROPHYSICS

Spectral evolution of nova V 443 Scuti 1989

G.C. Anupama[1,2], H.W. Duerbeck[3,4], T.P. Prabhu[1], and S.K. Jain[1]

[1] Indian Institute of Astrophysics, Bangalore 560034, India
[2] Inter-University Centre for Astronomy and Astrophysics, Post Bag 4, Ganeshkhind, Pune 411007, India
[3] Astronomisches Institut, Westfälische Wilhelms-Universität Münster, Wilhelm-Klemm-Str. 10, W-4400 Münster, Federal Republic of Germany
[4] European Southern Observatory, La Silla, Casilla 19001, Santiago 19, Chile

Received April 1, accepted May 11, 1992

Abstract. Spectroscopy of the moderately fast nova V443 Sct is presented, based on data obtained at the Vainu Bappu Observatory and at the European Southern Observatory. Observations were made during the brightness fluctuations following maximum, and during the transition stage. A few broadband polarimetric observations are also given. The spectrum and its evolution are similar to novae with the same type of light curves. The extinction $E_{B-V} = 0.4$ is derived from ratios of higher members of the hydrogen Balmer and Paschen series, a distance of 8.0 kpc is estimated from magnitude-decay time relations. Balmer line fluxes at late stages are used to derive the mass of the ejected ionized shell, $\sim 3.5 \cdot 10^{-5}\ M_\odot$. The variation of line flux is compatible with a homogeneous, completely filled shell whose density declines with time as $N_e \propto t_d^{-2}$ cm^{-3}, where t_d is the time in days since maximum, and whose temperature rises from 6000 to 17000 K in the 272 days following outburst. On day 77, the ionizing source had a size of $\sim 1\ R_\odot$ and a temperature of 9×10^4 K. During the nebular phase, the size decreased to $\sim 0.5\ R_\odot$ and the temperature rose to $\sim 2 \times 10^5$ K, while the luminosity appears to have remained constant for the first 236 days after outburst.

Key words: stars: variable – stars: novae – stars: V443 Sct

1. Introduction

Nova V443 Sct was discovered on 1989 September 20 by Wild (1989). Pre-discovery photovisual and photographic observations on September 6.85–8.65 and September 17.41–18.79 (McNaught 1989, Wenzel 1989) indicate that the nova was discovered in the post-maximum phase. The observations of Wenzel indicate that it was rising towards maximum on September 6–9. A pre-maximum halt must have been reached near September 9 at about visual magnitude 9. Maximum light is unfortunately not covered by sky patrol observations, since it occurred around full moon. The outburst light curve places V443 Sct among the moderately fast novae exhibiting marked oscillations near maximum light (type Bb in the classification scheme of Duerbeck 1981). Fig. 1 shows the light curve, based on magnitudes from IAU and AAVSO circulars. With its triple maximum peak, the light curve shows a cursory resemblance to that of DN Gem (see, e.g., Dokuchaeva 1958), and from this we estimate that maximum light was reached around September 14 at about visual magnitude 8. This extrapolated maximum brightness and the interpolated time of maximum (1989 September 14.0 = day 0 = JD 2 447 783.5) leads to a t_3-time of 46 ± 9 days, as compared to 37 days for DN Gem. Time intervals between subsequent maxima are also longer in V443 Sct than in DN Gem.

The averaged position of V443 Sct as determined by Wild (1989) and McNaught (1989) is R.A. $18^h46^m58\overset{s}{.}13$, Decl. $-6°14'45\overset{''}{.}2$ (1950.0). The nova field is crowded, making the identification of the prenova ambiguous. There is a very faint star, a south-eastern appendix to a bright one, at R.A. $18^h46^m58\overset{s}{.}13$, Decl. $-6°14'45\overset{''}{.}3$ (rms $\sim 0\overset{''}{.}3$) as measured visually on the J glass copy of the ESO/SERC sky survey with the ESO Optronics machine (Duerbeck 1992). Its estimated brightness is 21^m. Assuming this to be the prenova, we derive an outburst range of $\sim 13^m$. With a visual absorption $A_V = 1.2$ and a distance of 8 kpc, as determined in section 4.2, the absolute magnitude of the prenova is $M_V = 5.3$, which lies in the range of observed prenova brightnesses and gives confidence to the identification.

Rosino et al. (1991) describe in detail the spectral development of the nova from its early decline to the nebular phase. Williams et al. (1991) present CTIO spectra obtained during the same stages, and classify the spectra following the CTIO classification scheme. Huchra et al. (1989) briefly describe spectra taken on 1989 September 25. Here we discuss spectroscopic observations of the nova obtained between 1989 September 25 and December 4 at the Vainu Bappu Observatory (VBO), Kavalur, and at the European Southern Observatory (ESO), La Silla, as well as polarimetric observations made at VBO.

2. Observations

2.1. Spectroscopic observations at VBO

For spectroscopic observations at VBO the UAG spectrograph at the Cassegrain focus of the 1.02m telescope was used. Photographic spectra were taken between 1989 September 25 and October 3 with the 150 mm camera, a Varo 8605 image intensifier, and Kodak 103aD plates. They were calibrated with an auxiliary calibration spectrograph. During 1989 November and December, spectra were recorded using the 250 mm camera with CCD detector.

Send offprint requests to: H.W. Duerbeck, first address.

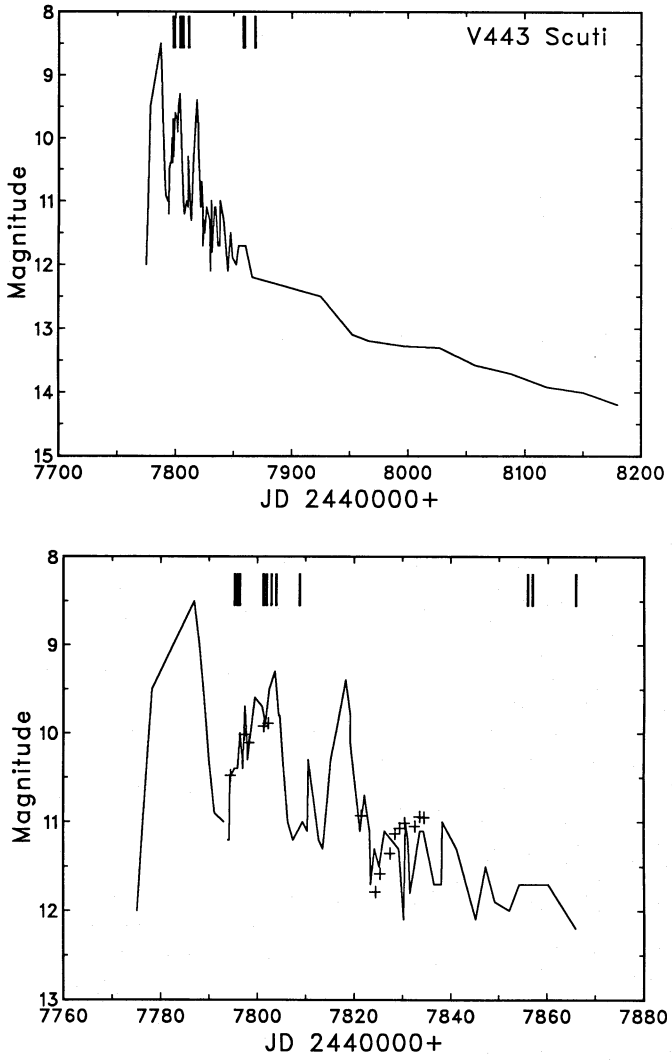

Fig. 1. The light curve of V443 Sct. Vertical bars indicate the epochs of spectroscopic observations, JD 2 447 780 = 1989 September 10.5. The total light curve available so far (top) and the early light curve (bottom) are shown separately. Photographic magnitudes measured until 1989 September 23, and visual estimates thereafter are connected by straight lines. Photoelectric V magnitudes during the early stages are indicated by '+'

The photographic spectra were digitized with a step width of 5 μm using the PDS 1010M microdensitometer at the Indian Institute of Astrophysics; they were Fourier smoothed using a low-pass filter with cutoff at 15 cycles mm^{-1}, and intensity-calibrated. The spectrophotometric standard stars HD 19445 and HR 8681 were used for photographic flux calibration. Zero point corrections to the observed fluxes were applied using VRI magnitudes reported in the IAU circulars.

The CCD data were individually de-biased and flat-field corrected, and one-dimensional spectra were extracted using the optimal extraction method by Horne (1986). HD 19445 was used for CCD flux calibration. Standard fluxes beyond 8300 Å were not available, hence, only an estimated correction for instrumental response was applied to the nova spectrum beyond 8300 Å, and the fluxes are somewhat uncertain.

All reductions were performed with the VAX 11/780 installation at VBO using the RESPECT software (Prabhu & Anupama 1991).

2.2. Spectroscopic observations at ESO

Spectroscopic observations at ESO were carried out with the Cassegrain spectrograph and CCD at the 1.52m telescope. Several spectrophotometric standards were observed in order to derive the instrumental response. The nova was observed through narrow as well as wide slits. The narrow-slit spectral fluxes were scaled to those of the wide-slit spectra in order to obtain well-resolved, flux calibrated spectra.

Two high-resolution spectra were obtained with the Coudé Echelle Spectrometer (CES), fed by the 1.4m Coudé Auxiliary Telescope (CAT), using a CCD detector. The slit was set to a resolution of 60 000. The spectra are not flux calibrated. All reductions were performed using ESO IHAP- and Muenster ADAS-software.

2.3. Polarimetric observations at VBO

Linear polarization of the nova was measured at VBO on 1989 October 7, 9 and 22–25. A star and sky chopping polarimeter was used at the Cassegrain focus of the 1.02m telescope. The polarimeter is described in detail by Jain & Srinivasulu (1991). A brief description of the instrument and the method of analysis is given here.

A photomultiplier-based photon counting system measures light, as a polaroid is rotated through 360° in steps of 1°.8. A sky chopper is used to measure star+sky and sky separately in each orientation (channel). The dwell time at each channel is 15 ms. Typically 80–90 such scans are obtained and co-added. The sky counts are subtracted from each channel, and the equation

$$I_i = I_0\ [1 + Q\cos 2\theta_i + U\sin 2\theta_i]$$

is fitted to the data by computing the moments $\langle I_0 \cos 2\theta\rangle$ and $\langle I_0 \sin 2\theta\rangle$. Instrumental polarization is determined, using observations of unpolarized standards obtained during the same night, and subtracted from the Q and U components. The zero point of the position angle is determined using observations of polarized standards of the same night.

On October 7 and 9 (days 23 and 25), the nova was observed in the V band only, because of the non-photometric sky. On day 23, the measured polarization was $(4.08 \pm 0.86)\%$ at PA $4° \pm 6°$ and on day 25 $(1.54 \pm 0.39)\%$ at PA $175° \pm 8°$. Observations were made in the V and R bands on October 22, 23 and 24 (days 38-40) with better skies. Although measurements were attempted in the B and I bands, the count rates are too low and the results unreliable. The mean polarization on these nights was $(0.65 \pm 0.41)\%$ in V at PA $167° \pm 19°$, and $(0.62 \pm 0.20)\%$ in R at PA $159° \pm 14°$. While measurements in the first two nights may be affected by cirrus, the later measurements may be interpreted as interstellar polarisation (see below).

3. The spectrum

The spectra of nova V443 Sct presented here cover four epochs:
(I) 1989 September 25–26 (days 11-12), at $m_{vis} = 10.5$, soon after maximum, when the nova was recovering from a local dip in the light curve;
(II) 1989 October 1–3 (days 18-20), at $m_{vis} = 9.5$, during a subsequent secondary maximum in the light curve;

Table 1. V443 Sct: Journal of observations

epoch	day after maximum	date 1989 UT	date JD 2447000+	range Å	resolution Å	telescope
I	11	Sep 25.00	749.50	3200 – 10500	8	ESO 1.52
	12	25.58	750.08	4500 – 8900	16	VBO 1.02
	12	Sep 26.06	795.56	Hα	0.1	ESO CAT
II	17	Sep 30.99	800.49	Hα	0.1	ESO CAT
	18	Oct 1.58	801.08	5000 – 8900	8	VBO 1.02
	18	1.62	801.12	4000 – 8000	8	VBO 1.02
	18	1.66	801.16	5000 – 8900	8	VBO 1.02
	18	1.69	801.19	4000 – 8000	8	VBO 1.02
	19	Oct 2.57	802.07	4000 – 8000	8	VBO 1.02
	19	2.60	802.10	5000 – 8900	8	VBO 1.02
	19	2.62	802.12	5000 – 8900	8	VBO 1.02
	20	Oct 3.56	803.06	5000 – 8900	8	VBO 1.02
	20	3.62	803.12	4000 – 8000	8	VBO 1.02
III	24	Oct 8.00	807.50	3200 – 7100	4	ESO 1.52
IV	72	Nov 24.57	855.07	6100 – 6800	2.6	VBO 1.02
	73	Nov 25.55	856.05	4500 – 7600	10	VBO 1.02
	73	25.57	856.07	4500 – 7600	10	VBO 1.02
	82	Dec 4.56	865.06	6100 – 9200	10	VBO 1.02
	82	4.58	865.08	6100 – 9200	10	VBO 1.02

(III) 1989 October 8 (day 24), at m_{vis} = 11.1, during a local minimum;
(IV) 1989 November 24, 25 and December 4 (days 72-73, 82), at $m_{vis} \sim 12.2$, during the smooth transition phase. The average composite spectrum of these observations will be quoted as that of "day 77".
Hα was observed at high resolution on September 26 and 30 (days 12 and 17).

Details of observations are given in Table 1. Dates are marked on the light curves in Fig. 1. Spectra are shown in Figs. 2–5.

The spectral continuum evolution during the light fluctuations after maximum closely follows the light curve. In fact, about 75% of the light variations can be explained by continuum variations. This suggests that the fluctuations in the light curve are caused primarily by variation of the photospheric radius.

At all epochs, the spectra show strong emission lines, characteristic of a nova spectrum during early decline. Tables 2 and 3 list the line identifications and observed fluxes relative to Hβ, as well as the observed flux of Hβ. The evolution of the emission line spectrum is similar to that of other novae of the same speed class, *e.g.*, LW Ser (Prabhu & Anupama 1987) and V1819 Cyg (Whitney & Clayton 1989).

The spectrum during the first three epochs resembles that of the diffuse enhanced stage, whereas the spectrum in the last epoch is that of the O I flash – Orion stage. These spectra complement the data presented by Rosino et al. (1991) and Williams et al. (1991). In the following, the spectral appearance at each epoch is briefly described.

Epoch I: The first two spectra were obtained with only 0.58 days time difference – one at VBO using the image tube spectrograph, another one at ESO. The flux-calibrated spectra agree very well. Discrepancies at a few wavelengths can be attributed to irregularities in the image-tube fiber-optics. The ESO spectrum is used for further analysis (Figs. 2 and 3).

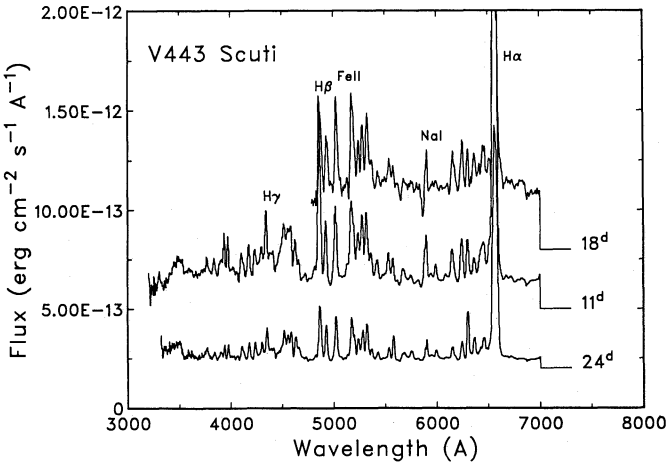

Fig. 2. Spectra of V443 Sct in the region 3200–7000 Å on 1989 September 25 (day 11, epoch I; middle), October 1–3 (days 18-20, epoch II; top) and October 8 (day 24, epoch III; bottom). Offsets of 0.5×10^{-12}, 0.8×10^{-12} and 0.2×10^{-12} in flux units are added to the spectra of the three epochs, respectively. The zero point is shown by the horizontal line at the right, together with the day number since maximum. Note that the continuum was brighter on day 18 than on days 11 and 24

The spectrum is dominated by strong broad emission lines (average FWHM $\sim$ 1700 km s^{-1}). P Cygni-absorptions are generally very weak, O I λ7774, however, shows an indication of P Cygni-absorption at −1270 km s^{-1}.

Epoch I-II, Hα profiles: The Hα line observed on days 12 and 17 at high resolution shows a structured profile (Fig. 4). The

Table 2. V443 Sct: Line identifications and observed fluxes relative to Hβ, in the region 3400–6000 Å.

λ_m Å	identification		flux relative to Hβ day 11	18	24	77
3450	3416.02	Fe II (16)				
	3494.67	Fe II (16)	0.424		0.563:	
	3456.93	Fe II (76)				
3593	3596.05	Ti II (15)	0.161		0.046:	
3716	3721.94	H_{14}	0.041			
3739	3734.37	H_{13}	0.040			
3763	3750.15	H_{12}	0.149		0.164	
	3770.63	H_{11}				
3840	3835.39	H_9	0.122		0.103	
3902	3889.05	H_8	0.144		0.131	
3937	3933.66	Ca II (1)	0.496		0.153	
3976	3968.47	Ca II (1)	0.163		0.174	
	3970.07	Hϵ				
4018	4012.37	Ti II (11)	0.094		0.079	
4109	4101.74	Hδ	0.165		0.259	
4175	4173.45	Fe II (27)	0.267		0.227	
4233	4233.17	Fe II (27)	0.170		0.253	
4302	4303.17	Fe II (27)	0.187		0.284	
4345	4340.47	Hγ	0.381		0.519	
	4351.76	Fe II (27)				
4386	4385.38	Fe II (27)	0.248		0.312	
4408	4416.82	Fe II (27)				
4529	4515.34,	4520.23,				
	4555.89	Fe II (37)				
+	4522.63	Fe II (38)	1.187	1.421	0.795	0.960
	4549.47	Fe II (38)				
4582	4583.83	Fe II (38)				
4635	4629.34	Fe II (37)	0.381	0.576	0.327	
	'4640'	N/O bld.				1.341
4864	4861.33	Hβ	1.000	1.000	1.000	1.000
4925	4923.92	Fe II (42)	0.272	0.879	0.553	0.557
5018	5018.43	Fe II (42)	0.427	1.400	0.767	1.354
	5005.14	N II (19)				
5172	5169.03	Fe II (42)	0.660	1.713	0.939	0.951
	5197.57	Fe II (49)				
5236	5234.62	Fe II (49)	0.242	0.635	0.295	0.170
5276	5275.99	Fe II (49)	0.377	0.847	0.493	0.414
5316	5316.61	Fe II (49)	0.402	1.151	0.590	0.615
	5316.78	Fe II (48)				
5365	5362.86	Fe II (48)	0.197	0.396	0.152	0.045
5423	5425.27	Fe II (49)	0.212	0.354	0.103	0.041
	5414.09	Fe II (48)				
5486	5495.70,	5480.10,	0.103	0.283	0.022:	0.173
	5462.62	N II (29)				
5533	5534.86	Fe II (55)				
	5530.27	N II (63)	0.223	0.211	0.451	0.119
	5535.39	N II (63)				
5577	5577.35	[O I] (3)	0.193	0.324	0.341	0.398
5680	5666.64,	5676.02,				
	5679.56,	5686.21,	0.210	0.191	0.200	0.956
	5710.76	N II (3)				
5755	5754.80	[N II] (3)	0.053	0.171	0.208	1.636
5903	5889.95	Na I (1)	0.263	0.380	0.257	1.248*
	5895.92	Na I (1)				
5945	5941.67	N II (28)	0.039	0.072	0.058	
5989	5991.38	Fe II (46)	0.084	0.139	0.144	0.221
	5995.28	O I (44)				
$F_{H\beta}$ (10^{-11} erg cm^{-2} s^{-1})			2.804	1.102	0.839	0.226

*Contribution from He I 5876 and N II 5942.

Table 3. V443 Sct: Line identifications and observed fluxes relative to Hβ, in the region 6000 Å – 1.1 μm.

λ_m Å	identification		flux relative to Hβ day 11	18	24	77
6084	6084.11	Fe II (46)	0.041	0.023	0.020	
6152	6155.99,	6156.78,				
	6158.19	O I (10)	0.214	0.648	0.220	0.203
	6147.74	Fe II (74)				
6247	6247.56	Fe II (74)	0.235	0.711	0.263	0.104
6303	6300.23	[O I] (1)	0.226	0.444	0.775	1.748
6365	6363.88	[O I] (1)				
	6416.91	Fe II (74)	0.144	0.571	0.396	1.115
	6347.09	Si II (2)				
	6371.36	Si II (2)				
6455	6456.38	Fe II (74)				
	6453.64,	6454.48,	0.428	0.560	0.496	0.889
	6456.01	O I (9)				
6563	6562.82	Hα	10.895	12.701	7.144	15.695
6676	6678.15	He I (46)	0.032	0.077		0.065
6827	6812.26	N II (54)	0.023	0.103	0.010	
	6836.2	N II (54)				
7069	7065.19	He I (10)	0.014	0.012		0.121
7114	7112.36,	7115.13,	0.033	0.056		
	7119.45	C II (20)				
7136	7135.8	[A III] (1)		0.087		0.145
7224	7222.39	Fe II (73)				
	7231.12	C II (3)	0.090	0.282		0.304
	7236.19	C II (3)				
7317	7307.97	Fe II (73)	0.181	0.189		
	7320.70	Fe II (73)				
	7319.92	[O II] (2)				1.456
	7330.19	[O II] (2)				
7457	7462.38	Fe II (73)	0.306	0.746		0.329
7778	7771.96,	7774.18,	1.006	1.729		0.289
	7775.40	O I (1)				
7884	7877.13	Mg II (8)	0.065	0.465		0.145
	7896.37	Mg II (8)				
8217	8184.80,	8187.95,				
	8216.28,	8223.07,	0.448	1.229		0.895
	8242.34	N I (2)				
8446	8446.35	O I (4)	1.864	4.139		6.679
	8446.76	O I (4)				
8502	8498.02	Ca II (2)	1.391	3.238		
	8502.49	P_{16}				
8541	8542.09	Ca II (2)	1.539	3.420		
	8545.38	P_{15}				
8602	8594.01	N I (8)	0.085	0.213		0.644
	8598.39	P_{14}				
8663	8662.14	Ca II (2)	1.494	2.283		
	8665.02	P_{13}				
8717	8703.24,	8711.69,	0.039			2.417
	8718.82	N I (1)				
8857	8862.79	P_{11}	0.073			
9065	9060.6	N I (15)	0.395			
9239	9228.11	S I (1)	0.685			
	9237.49	S I (1)				
9400	9405.77	C I (9)	0.286			
9545	9545.97	P_8	0.151			
10026	9999	Fe II	0.339			
	10049.38	P_7				
10116	10113.4	N I (18)	0.085			
$F_{H\beta}$ (10^{-11} erg cm^{-2} s^{-1})			2.804	1.102	0.839	0.226

line has a FWHM of ~ 1700 km s^{-1} at the earlier date, later it narrowed to ~ 1500 km s^{-1}. Several sharp lines can be attributed to telluric absorption. Two blueshifted absorption features are present on days 12 and 17 after maximum, on the first date at -1010 and -660 km s^{-1}, on the second one at -950 and -680 km s^{-1}. They are very weak in the first spectrogram. Both components belong to the principal spectrum. Diffuse enhanced lines, observed by Rosino et al. (1991), are outside the covered spectral range.

The emission line profiles bear some resemblance to the typical four-peaked structure, also observed in other novae, indicating a polar blob/equatorial ring structure. The central emission peaks, separated by a weak dip, lie at $+20$ and -130 km s^{-1} in the earlier spectrum, and at $+80$ and -80 km s^{-1} in the later spectrum. The red emission peak is at $+450$ and $+390$ km s^{-1}, respectively, and the blue emission peak is markedly depressed in both spectra. Since at no time dust formation is obvious, self-absorption in an expanding system of optically thick clouds, where the approaching clouds have their ionized parts away from the observer, can explain the profile (Ferland, Netzer & Shields 1979).

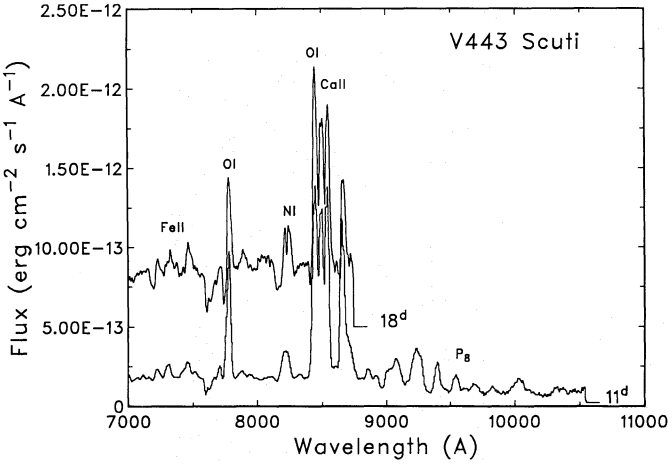

Fig. 3. Spectra of V443 Sct in the region 7000–10500 Å on September 25 (day 11, epoch I; bottom) and October 1–3 (days 18-20; epoch II, top). Offsets of 0.2×10^{-12} and 0.5×10^{-12} in flux units are added to the two spectra, respectively. The zero point is shown by the horizontal line at the right of each spectrum, together with the day number since maximum. Note that the continuum was brighter on day 18-20 compared to day 11

The central emission decreased with time, relative to the red and blue emission peaks. This is similar to the behaviour observed in HR Del (Seitter 1971, Hutchings 1972), and suggests that the outer emission peaks may originate in a (non-uniform) equatorial ring seen almost edge-on (Soderblom 1976). Since this conclusion is based on only two profiles of a single line, it must be regarded as preliminary. It reminds us, however, of the fact that the conclusions drawn from low-dispersion line strengths refer only to crude average conditions in well-structured shells.

Epoch II: The continuum level is clearly higher than at epoch I. At the same time, the nova became brighter by 1.2 magnitudes (see Fig. 1). The observed increase in the continuum level by $0^m.9$ accounts for most of the rise in visual magnitude, the increase in total emission line strengths accounts for the remainder. The P Cygni-absorptions have become stronger, as is most clearly seen in Na I and O I (Figs. 2 and 3). Hα has an absorption

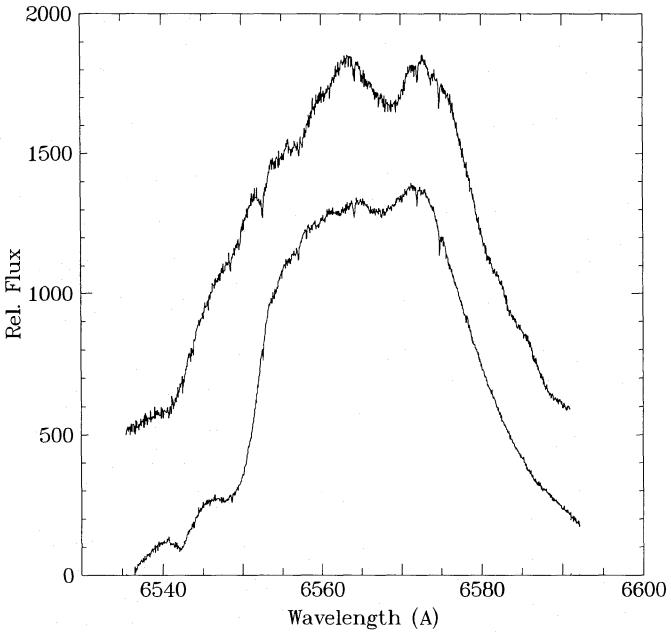

Fig. 4. Hα profiles of V443 Sct on September 26 (day 12; top, shifted by 500 units) and on September 30 (day 17; bottom)

velocity of -1580 ± 40 km s^{-1}, whereas the mean velocity obtained from Na I, Fe II and O I is -1300 ± 90 km s^{-1}.

Between epochs II and III, Rosino et al. (1991) observed a value of -1500 km s^{-1} for Hα and values ranging from -1300 to -1630 km s^{-1} for other lines, which they attribute to the diffuse-enhanced absorption system. They also measured the principal absorption system at -700 km s^{-1}.

Epoch III: The continuum level has decreased by about $2^m.3$, corresponding to 2^m in the light curve (Fig. 1). The lines of H, Fe II and Na I D have also decreased. [O I] λ6300 has become quite prominent.

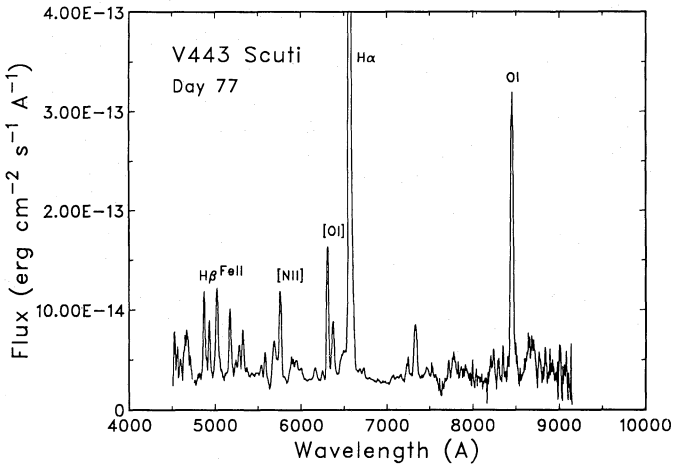

Fig. 5. Composite spectrum of V443 Sct, November 25, 26 and December 4 (days 72-82, epoch IV), in the region 4500–9200 Å

Epoch IV: The nova is now in the O I–Orion stage (Fig. 5), near the end of the transition stage of the light curve. The continuum level has decreased further. Hα/Hβ has grown considerably.

[O II] $\lambda\lambda$ 7320-7333 and [N II] $\lambda\lambda$ 5755, as well as the emergence of the 4640 feature indicate an increase in ionization. The O I λ 8442 line is strongly amplified relative to O I λ 7774 by Lyβ fluorescence.

Using the CTIO classification (Williams et al. 1991) the spectral evolution of V443 Sct during the four epochs covered by our observations can be described as follows. The spectrum on days 11-24 is dominated by permitted lines (P). During all phases the Fe II lines of multiplet 42 are quite strong relative to Hβ, ranging from about half the intensity of Hβ to a higher flux in Fe II λ 5018 than in both Hβ and [N II] λ 5755. The latter is also evident in Rosino et al.'s spectrum of day 64, taken at higher resolution. The spectrum thus merits the subscript fe.

O I λ8446 is always stronger than Hβ, so that the superscript o is applicable. According to the classification scheme of Williams et al., the nova is of type P^{o}_{fe} throughout our observations.

In the spectra of days 64 and 77, the Fe II λ5018 line appears clearly broader than the unblended Hβ line, and blending with N II $\lambda\lambda$4991-5040 (as is also found in V1819 Cyg, Whitney & Clayton 1989) and possibly [O III] λ5007 cannot be excluded. We thus conclude that either this phase is a transition between P and A or the Fe II lines are unusually strong in V443 Sct, making the classification ambiguous, even after phase A has been reached. Considering the fact that the nova has now declined by more than 4^{m} and left the transition phase, the latter appears to be more likely. The evolution may thus be described as

$$P^{o}_{fe} \rightarrow A^{o}_{o}$$

Later observations: The observations of Rosino et al. (1991) in the nebular stage, 236 days after outburst, as well as those of Williams et al. (1991), 229 and 375 days after outburst, can still be classified as A_o.

4. Analysis and discussion

4.1. Absolute magnitude

The light curve of V443 Sct (Fig. 1) indicates that the maximum was reached around September 14, 1989 (JD 2447783.5). From the resemblance of the fragmentary light curve with that of DN Gem, it is estimated that the maximum magnitude was $V_{max} = 8.0$ (see introduction). Rosino et al. (1991) suggest a maximum value of $V_{max} \sim 7.5$ on September 13 – 14.

A smooth fit to the light curve through the oscillations between maximum and early decline gives the following parameters: (i) magnitude at 15 days from maximum (1989 September 29 = JD 2447798.5): $V_{15} = 10.0$, (ii) time of decline through 2 magnitudes in V: $t_2 = 16 \pm 5$ days, (iii) time of decline through 3 magnitudes in V: $t_3 = 46 \pm 9$ days. With these parameters, the absolute magnitude of the nova at maximum can be estimated using various ($M_{V,max}, t_{decline}$)-relations. The results are listed in Table 4. The values range from $M_V = -7.2$ to $M_V = -8.3$ with the unweighted mean

$$M_V = -7.8 \pm 0.4.$$

This yields the uncorrected distance modulus

$$(m - M) = 15.8 \pm 0.5.$$

4.2. Reddening and distance

The foreground reddening towards V443 Sct is estimated using various indicators and relations.

4.2.1. Polarization

The average polarization of the nova on days 38-40 was $p_V = 0.65 \pm 0.41$ %. Assuming this to be totally interstellar in origin, one obtains the lower limit $E_{B-V} \geq p/9.0 = 0.07$ (Serkowski et al. 1975).

4.2.2. Line ratios

Reddening may be estimated by comparing theoretical and observed flux ratios of recombination lines, which are well separated in wavelength. The He I ratio 5876/4471 is not sensitive to radiative transfer effects and could be used, although the estimate is uncertain because of the small baseline. While He I lines are not clearly present in our spectra, the ratio found by Rosino et al. (1991) at later stages leads to a rough estimate: $E_{B-V} = 0.24$ (+0.16,−0.20).

During the early phases of the outburst, the density in the envelope is high and the Balmer line ratios, especially of the lower series members, are affected by radiative transfer effects. For this case, reliable theoretical recombination line ratios are not available. The higher members of the Balmer and Paschen series are less affected and may be compared with theoretical values. When the nova enters the nebular phase, the envelope density becomes sufficiently small so that the Balmer line ratios approach Case B values.

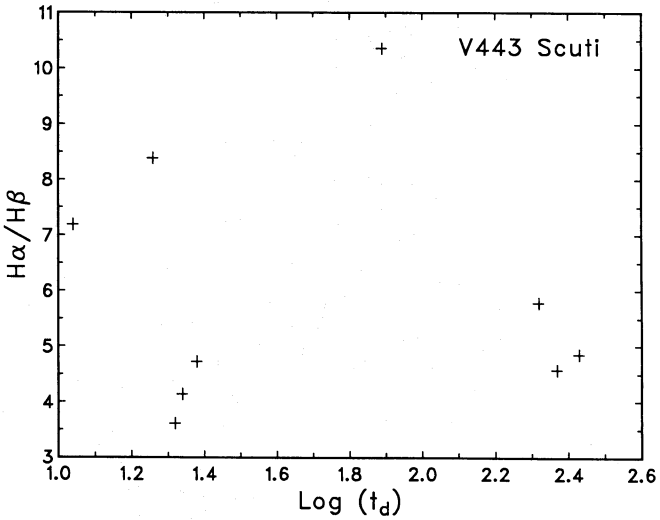

Fig. 6. De-reddened Hα/Hβ ratio versus time since maximum (in days)

During our observations, V443 Sct showed Hα/Hβ ratios which varied between 3.5 and 10 (Fig. 6, see Sect. 4.3.1), indicating that they are affected by radiative transfer effects. The spectrum obtained on day 11 shows the lines P_8, P_{11}, H_{13} and H_{14} with no severe blending from other lines. Comparing the ratios of H_{13}/P_8 and H_{14}/P_{11} with calculated ratios from the tables of Hummer & Storey (1987) for $T_e = 10^4$ K, $N_e = 5 \times 10^9$ cm^{-3} (values to be justified in Section 4.3.3), the reddening from both ratios is $E_{B-V} = 0.41 \pm 0.03$.

4.2.3. Colour index

Photometry of the nova by Monella (1989) gives the colour indices B − V = +0.21 on day 15, B − V = +0.27 on day 18 and B − V = +0.21 on day 19; the average value at approximately 2

Table 4. V443 Sct: Absolute magnitude estimates.

relation	ref.	M_V(max)
$M_B(\max) = -10.67 + 1.80 \log t_3$ $\pm 0.30 \quad \pm 0.20$	1	-7.9 ± 0.8(*)
$M_V(\max) = -10.70 + 2.41 \log t_2$ $\pm 0.30 \quad \pm 0.23$	2	-7.8 ± 0.9
$M_V(t_{15}) = -5.60 \pm 0.45$	2	-7.6 ± 0.5
$M_V(t_{15}) = -5.23 \pm 0.39$	3	-7.2 ± 0.4
$M_V(\max) = -7.89 - 0.81 \arctan\left([1.32 - \log t_2]/0.19\right)$	4	-8.3 ± 0.4

1: Pfau (1976), 2: Cohen (1985); 3: van den Bergh & Younger (1987);
4: Capaccioli et al. (1989).
* assuming $(B-V)_0 = 0.2$ at maximum.

magnitudes below maximum is $+0.23 \pm 0.03$. For several novae at two magnitudes below maximum, van den Bergh & Younger (1987) find the unreddened index $(B-V)_0 = -0.02 \pm 0.12$. The observed B − V-colour thus implies $E_{B-V} = 0.25$ for V443 Sct. The error margins are large, and the observed colours of the nova corrected for $E_{B-V} = 0.41$ (from section 4.2.2.) give $(B-V)_0 = -0.18$ and $(U-B)_0 = -1.09$, which is still within the range of intrinsic colours of novae two magnitudes below maximum.

4.2.4. Reddening

The well-studied globular cluster M11 (= NGC 6705) lies 21′ east of V443 Sct. The cluster has the apparent distance modulus $(m-M) = 12.7$ (Lee et al. 1989) and reddening $E_{B-V} = 0.44$ (Anthony-Twarog et al. 1989), yielding a distance of 1.8 kpc. Assuming the reddening per kpc to be $0.44/1.8 = 0.24$ along the line of sight, the uncorrected nova distance modulus (see Sect. 4.1) gives the distance 3.8 kpc and $E_{B-V} = 0.9$. The scale height of dust in the Galaxy, however, is about 120 pc, and the ray of vision to the nova (galactic latitude $b = -3°.3$) leaves the dust plane and the Aquila-Carina arm at about 2 kpc. No substantial reddening is expected beyond this distance, and the above reddening estimate is an upper limit, the distance a lower limit. The nova may thus belong to the central bulge of the Galaxy.

4.2.5. Summary of reddening and distance estimates

(a) Polarization: $E_{B-V} \geq 0.07$
(b) Line ratio: $E_{B-V} = 0.41$
(c) B − V colour: $E_{B-V} \geq 0.25$
(d) Reddening per kpc: $d \geq 3.8$ kpc, $E_{B-V} \leq 0.9$.

Only (b), in combination with the absolute magnitude estimate from the light curve decay times, yields definitive values: the corrected distance modulus $(m-M)_0 = 14.5$ and the distance $d = 8.1$ kpc, in accordance with the limits of (d). Rosino et al. (1991) give $E_{B-V} = 0.30$, based on the average colour index of the nova during early decline. With their estimate of $V_{max} = 7.5$ and $M_V^{max} = -7.8$, this yields the distance $d \sim 7.6$ kpc. The values of reddening and distance given here are thus in rough agreement with their results. In the following, a reddening correction $E_{B-V} = 0.4$ and the distance $d = 8.0$ kpc are assumed.

4.3. *Physical conditions*

4.3.1. Optical depths in hydrogen emission lines

The observed, reddening-corrected ratios Hα/Hβ are plotted in Fig. 6. The measurements of Rosino et al. (1991) are also included. All ratios are considerably higher than the theoretical value for Case B, but they can be produced with high densities and large optical depths in Lyα and Hα. Comparison of the observed Hα/Hβ ratios with the theoretical models of Netzer (1975), Krolik & McKee (1978) and Drake & Ulrich (1980) indicates an optical depth of Lyα in the range $\tau =$ several 10^5–10^6 and an optical depth of Hα in the range 100–10 during the phases of outburst covered by observations. The ratios Hβ/Hγ and Hγ/Hδ also indicate large optical depth in Lyα. The smaller Hα/Hβ ratio in the early days and weeks of the outburst may be explained by collisional de-excitation of the $n = 3$ level, but the required densities are quite high.

The evolution of the Hα/Hβ ratio (small → large → small, and approaching case B) appears to be a general signature of nova outbursts. It was observed in the very fast nova V1500 Cyg, where the maximum of the ratio was reached on day 20 (Ferland, Netzer & Shields 1979), in the fast nova V446 Her, where it was reached on day 40 (Meinel 1960) as well as in the slow nova V1819 Cyg, where it was reached on day 92 (Whitney & Clayton 1989). The maxima approximately coincide with the occurrence of the fluorescence effect of Lyβ, producing an unusually strong O I λ8446 emission. In V443 Sct, it occurred around day 77.

4.3.2. Temperature

During the initial outburst stages when the densities in the line-forming region are relatively high, the ratio of [O I] λλ 5577/6300 can be used to determine the temperature from the relation

$$[\text{O I}]\ 5577/6300 = 43 \exp\left(-2.58 \times 10^4 / T_e\right)$$

(Martin 1989).

The observed reddening-corrected ratio of [O I] 5577/6300 varied from 0.98 on day 11 to 0.37 on day 77, yielding a temperature variation from 6800 K to 5400 K. The mean temperature during the period of our observations is 6100 K. This value is consistent with that expected for a photoionized gas at high densities (Martin 1989).

Auroral and nebular lines of [NII] and [OIII] are visible in Rosino et al.'s spectra of days 236 and 272. Blending with

Balmer lines makes the line fluxes somewhat uncertain, but we find consistent solutions of $T_e = 17000$ K and $2.7 \cdot 10^6$ cm^{-3} (day 236) and $T_e = 17000$ K and $1.6 \cdot 10^6$ cm^{-3} (day 272). The weak, but persistent occurrence of [O I] 6330, 6363 at days 236 and 272 indicates that high density still prevails in small parts of the shell.

4.3.3. Shell mass and temporal variation of density

The physical parameters of days 236 and 272 after outburst may serve as a starting point in the derivation of the mass M of the nova shell. If we assume case B, we can write (Anderson and Gallagher 1977)

$$M = \frac{L_{H\beta}\,\mu\, m_H}{N_e} \left(\frac{4\pi\, j_{H\beta}}{N_e N_p} \right)^{-1}$$

where μ is the mean molecular weight, m_H the mass of the hydrogen atom, and the expression in brackets the volume emissivity. Inserting the Hβ luminosities $L_{H\beta}$ of 2.65 and $1.12 \cdot 10^{34}$ erg s^{-1}, and an emissivity of $7.9 \cdot 10^{-26}$ for 17 000 K and the derived electron densities for case B, shell masses of the order of 10^{-4} $M_\odot$ are obtained. However, if the occupied volume of such a mass with the assumed density is calculated, it is somewhat larger than the volume calculated from the velocity 750 km s^{-1} of the ejected shell, as derived from the FWHM of the emission lines (Sect. 3 and Rosino et al. 1991 – we conjecture that their "expansion velocity" of 1500 km s^{-1} was derived from the total line width).

Since at the assumed density case B is not yet strictly fulfilled, the emissivities of Hα and Hβ from Hummer & Storey (1987) for $T_e = 17\,000$ K and $N_e = 10^6$ cm^{-3} lead to revised masses of 2.9 and $2.1 \cdot 10^{-5}$ $M_\odot$ for $H\beta$ and to 5.2 and $4.1 \cdot 10^{-5}$ $M_\odot$ from $H\alpha$. The average value for the mass, $3.5 \cdot 10^{-5}$ $M_\odot$, now leads to an occupied volume which is very close to that occupied by the expanding shell.

Since there is almost no high resolution spectroscopy available to study the behaviour of different parts of the shell, it remains to see if our simplistic model, a shell homogeneously filled with matter, can explain the temporal behaviour of the Balmer emission lines (the structured appearance of the Balmer lines and the persistence of [O I] at late stages indicates that such a model is only a coarse approximation). Such a shell can be envisaged to be formed by a mass loss at constant velocity, decreasing with t^{-2}. The density in the expanding shell also decreases as t^{-2} and has the same value everywhere inside the shell. Balmer line fluxes f under case B conditions depend on volume V and density N_e as Vn_e^2, i.e. $f \propto t^3 t^{-4} \propto t^{-1}$. Analysis of the temporal decline of the Hα and Hβ fluxes yields exponents of -1.24 ± 0.1 and -1.21 ± 0.14. At early times, the lower Balmer series lines have large optical thickness, and major parts of the envelope are not yet ionized, thus leading to a less negative slope than the theoretical one, contrary to observations. However, the lower shell temperature at early times might well overcompensate these effects and lead to the observed dependence. Because of the scarceness of indicators of temperature and density at early times, it is difficult to develop an improved model that reproduces the observations in a unique way.

4.3.4. Helium abundance

The He I line fluxes may be used to estimate the relative numbers of singly ionized helium $N(He^+)/N(H)$ in the ejecta using standard techniques. On day 77, He I λ6678 was weakly present, also He I λ5876, though blended with Na I D. He II lines are not easily detectable in the spectra. This, together with the fact that He I lines are still weak indicates that ionization in the ejecta is still low and most of the helium is in neutral form.

Because of the blending of He I λ5876, only λ6678 is used to determine the He^+ abundance from the ratios 6678/Hβ and 6678/Hα. With emissivities for Hα and Hβ taken from Hummer & Storey (1987), for He I λ6678 from Brocklehurst (1972), at $T_e = 10^4$ K and $N_e = 10^7$ cm^{-3}, and the He I emissivity correction for collisional effects according to Clegg (1987), Hβ and Hα yield values $N(He^+)/N(H)$ of 0.15 and 0.04, respectively. Under the conditions of high optical depth in the envelope considered here, the ratio derived from Hβ gives an upper limit and that from Hα a lower limit (Whitney & Clayton 1989).

Adopting the model by Drake & Ulrich (1980) for $\tau(Ly\alpha) = 10^6$, $N_e = 10^8$ and $T_e = 10^4$, which has a similar Balmer decrement as the one observed on day 77, and using their emissivities for Hα and Hβ, we obtain $N(He^+)/N(H) = 0.043$ from Hβ and 0.054 from Hα.

A more reliable value for the helium abundance can only be derived by analyzing the later stages of the outburst, when most of the helium is ionized.

Rosino et al. (1991) derive for the nebular phase a helium abundance $N(He)/N(H) = 0.23$ from Hβ and 0.12 from Hα, using the He I $\lambda\lambda$4471, 5876 and 6678 emissivities uncorrected for collisional effects. After application of this correction, the revised abundance of He II is 0.11 from Hβ and 0.05 from Hα. The He II λ4686 flux gives $N(He^{++})/N(H) = 0.02$ (Hβ) and 0.01 (Hα). The revised total helium abundance is $N(He)/N(H) = 0.13$ (Hβ) and 0.06 (Hα), assuming there is no neutral He.

The He I λ6678 line gives a higher value for the abundance than the others. Rosino et al. attribute this to a possible blend line. The abundance estimated from this line does not change much when the correction for collisional effects is made. Clegg (1987) recommends the use of this line for He abundance determinations, since collisional effects are minimal. Using only the He I λ6678 line, the revised total helium abundance is 0.24 (Hβ) and 0.10 (Hα).

4.3.5. The central ionizing source

Using the He I and hydrogen line ratios, the Zanstra temperature T_* of the ionizing source may be estimated (Osterbrock 1989). The radius of the ionizing source may be estimated from the hydrogen line flux (Anupama & Prabhu 1989), as well as from the continuum.

The absence of He I in the early phases and of highly ionized lines later on indicates that the central ionizing source has not yet reached very high temperatures during the time of our observations.

On day 77, the presence of He I lines, although weak, indicates that the temperature of the source is $\gtrsim 10^4$ K. Using the reddening corrected He I λ6678/Hβ ratio, the Zanstra temperature $T_* = 8.7 \times 10^4$ K is derived. The radius of the source is 1.15 $R_\odot$, as determined from the Hβ flux, the Hummer & Storey (1987) emissivities, a covering factor of $\delta = 0.1$ (defined as the fraction of ionizing radiation intercepted by the nebula), and the assumed distance of 8 kpc.

The de-reddened continuum at 6000 Å is 7.8×10^{-14} erg cm^{-2} s^{-1} Å^{-1}, which has to be corrected for the superimposed nebular continuum. An estimate of the nebular continuum is made from $N_e N_H \gamma_\nu(H^0, T) V/(4\pi d^2)$. The emission coefficient γ_ν is listed by Osterbrock (1989). In terms of the shell mass M_{H^+},

obtained from the hydrogen line fluxes, the hydrogen continuum flux can be expressed as $M_{H^+} N_e \gamma_\nu / (4\pi m_H d^2)$. The stellar continuum flux thus corrected is 6.4×10^{-15} erg cm^{-2} s^{-1} Å^{-1}. At a temperature of 8.7×10^4 K, this corresponds to a radius of 4.7 $R_\odot$, assuming blackbody radiation.

The TNR model of nova outbursts (see, e.g., Starrfield et al. 1985) predicts that during the constant bolometric luminosity phase the effective temperature of the ionizing source increases, while the effective radius decreases, according to $T_{\rm eff} = 9 \times 10^4 R^{-1/2}$ (Williams 1991). This implies a radius of $\sim 1\ R_\odot$, in agreement with the value obtained from the emission line flux. The assumed covering factor thus appears to be reasonable, but the nebular continuum radiation appears to be much larger than expected.

During the nebular stage, about 250 days after maximum, Rosino et al. (1991) estimate the mean effective temperature $T_{\rm eff} \approx 1.83 \times 10^5$ K from the average ratio He II 4686/He I 5876. The radius at this temperature is 0.13 $R_\odot$, as obtained from the Hβ flux, assuming the covering factor 0.1. The continuum at 5000 Å, taken from Rosino et al.'s observation on JD 2 448 020, dereddened and corrected for nebular emission, yields a radius $R = 0.51\ R_\odot$, whereas the theoretically expected radius at this temperature is 0.24 $R_\odot$. Apparently the covering factor has decreased below 0.1, and the continuum emission is approaching that of a blackbody.

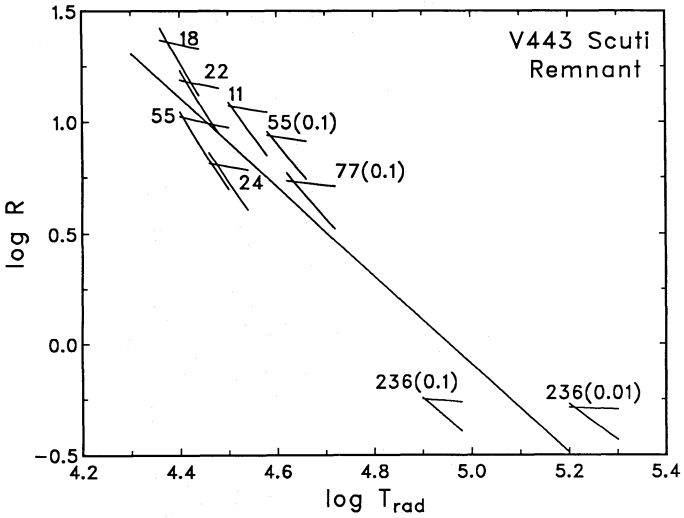

Fig. 7. The loci of continuum fluxes, corrected for nebular emission (nearly horizontal curves), and Hα emission line fluxes (steeper curves) arising from radiative recombination due to the blackbody source of radius R (in $R_\odot$) and temperature $T_{\rm rad}$ (in K) on different days after outburst. The continuum fluxes are based on our observations at 6000 Å except on days 22 and 236 where they are read from figures of Rosino et al. (1991) at 5000 Å. The day since outburst is indicated for each set of curves. The assumed covering factor is shown in parentheses whenever it differs from unity. The theoretical constant luminosity relation is shown as a straight line

Before day 77, the Zanstra temperature of the source could not be determined from our observations. Using, however, the fact that the continuum provides an upper limit to the radius and the emission line flux a lower limit, the loci of observed fluxes on all days covered by our and Rosino et al.'s observations are plotted, together with the theoretical relation, in the ($\log T_{\rm rad}$, $\log R$) diagram (Fig. 8). We conclude that the observations are in general agreement with the theoretical model, and that the covering factor decreases with time, because less radiation is intercepted.

Secondary peaks in the light curve occurred around day 17, day 35, day 52 and possibly also on day 77. It appears from the figure that spectra taken around the time of secondary peaks (i.e. on day 18 and 55) show an increase in the radius of the source contributing to the optical continuum.

Such a behaviour can also be studied when temperatures and radii of novae during outburst are derived from multicolour photometry (Duerbeck & Seitter 1979); photometry usually yields a better temporal resolution, but the disturbing influence of emission lines is difficult to remove.

If the mass-loss rate is not a monotonously decreasing function with time, secondary maxima of mass loss lead to a temporary growth of the quasi-photosphere and to visual maxima in the light curve, while the bolometric luminosity remains constant. The larger ratio of the size of the photosphere and that of the ejected shell in these maxima also leads to a strengthening of the P Cygni-absorption features, as is most clearly seen in the spectrum of day 18.

5. Conclusions

Spectra in the declining stages of nova V443 Sct are classified and analyzed. Interstellar reddening, luminosities, temperatures and helium abundance are derived. The observations can be described in terms of a central object radiating at constant luminosity, which emerges as its thick wind-type mass loss decreases with time as $\dot{M} \propto t^{-2}$.

Fluctuations in the mass loss rate can explain the irregular light curve and the spectral variations observed during early decline. High resolution spectroscopy indicates that the structure of the nova shell can be described by an equatorial ring and polar blobs. Despite the irregular mass loss rate and the fine structures in the lines, the density decline mimics that of a homogeneous expanding spherical shell, whose temperature gradually rises and which becomes almost completely ionized after 250 days.

Acknowledgements. This work forms part of the Ph.D. thesis of GCA, submitted to Bangalore University. GCA thanks the director of the Indian Institute of Astrophysics, for the facilities provided. HWD thanks the European Southern Observatory for support through their Senior Visitor programme, and the German-Israeli Foundation for Research and Development under grant I-133-109.7/89. He also acknowledges help from Ch. Gouiffes, Th. Augusteijn and R. Hanuschik, during whose observing runs the ESO observations were carried out. We also thank W. Seitter for useful comments on the manuscript, and R.E. Williams for assistance with the CTIO classification scheme.

References

Anderson, C.M., Gallagher, J.S. 1977, PASP 89, 264
Anthony-Twarog, B.J., Payne, D.M., Twarog, B.A. 1989, AJ 97, 1048
Anupama, G.C., Prabhu, T.P. 1989, JA&A 10, 237
Brocklehurst, M. 1972, MNRAS 157, 261
Clegg, R.E.S. 1987, MNRAS 229, 31p
Cohen, J.G. 1985, ApJ 292, 90
Dokuchaeva, O.D. 1958, Per. Zv. 12, 358
Drake, S.A., Ulrich, R.K. 1980, ApJS 42, 351
Duerbeck, H.W. 1981, PASP 93, 165

Duerbeck, H.W. 1992, Space Sci. Rev. (in preparation)
Duerbeck, H.W., Seitter, W.C. 1979, A&A 75, 297
Ferland, G.J., Netzer, H., Shields, G.A. 1979, ApJ 232, 382
Horne, K. 1986, PASP 98, 609
Huchra, J., Olowin, R., Layden, A. 1989, IAU Circ. 4862
Hummer, D.G., Storey, P.J. 1987, MNRAS 224, 801
Hutchings, J.B. 1972, MNRAS 158, 77
Jain, S.K., Srinivasulu, G. 1991, Opt. Eng. 30 (in press)
Krolik, J.H., McKee, C.F. 1978, ApJS 37, 459
Landolt, A. 1989, IAU Circ. 4862
Lee, C.W., Mathieu, R.D., Latham, D.W. 1989, AJ 97, 1710
Martin, P.G. 1989, in Classical Novae, eds. M.F. Bode & A. Evans, John Wiley, Chichester, p. 73
McNaught, R. 1989, IAU Circ. 4862
Meinel, A.B. 1963, ApJ 137, 834
Monella, R. 1989, IAU Circs. 4868, 4873
Netzer, H. 1975, MNRAS 171, 395
Osterbrock, D.E. 1989, Astrophysics of Gaseous Nebulae and Active Galactic Nuclei, University Science Books, Mill Valley
Pfau, W. 1976, A&Ap 50, 113
Prabhu, T.P., Anupama, G.C. 1987, JA&A 8, 369
Prabhu, T.P., Anupama, G.C. 1991, Bull. astr. Soc. India 19, 97
Rosino, L., Benetti, S., Iijima, T., Rafanelli, P. 1991, AJ 101, 1807
Seitter, W.C. 1971. IAU Coll. 15, Veröff. Remeis-Sternw. Bamberg 9, No. 100, 268
Serkowski, K., Mathewson, D.S., Ford, V.L. 1975. ApJ 196, 261
Soderblom, D. 1976, PASP 88, 517
Starrfield, S., Sparks, W.M., Truran, J.W. 1985, ApJ 291, 13
van den Bergh, S., Younger, P.F. 1987, A&AS 70, 125
Wenzel, W. 1989, IAU Circ. 4868
Whitney, B.A., Clayton, G.C. 1989, AJ 98, 297
Wild, P. 1989. IAU Circ. 4861
Williams, R.E. 1991, in IAU Coll. 122, Physics of Classical Novae, eds A. Cassatella & R. Viotti, Springer, Berlin, p. 215
Williams, R.E., Hamuy, M., Phillips, M.M., Heathcote, S.R., Wells, L., Navarrete, M. 1991, ApJ 376, 721

This article was processed by the author using Springer-Verlag LaTeX A&A style file 1990.